Physics – Uspekhi **64** (4) 344 – 356 (2021)

REVIEWS OF TOPICAL PROBLEMS PACS numbers: **61.50.–f**, 75.10.Jm, **75.25.–j**

Francisites as new geometrically frustrated quasi-two-dimensional magnets

M M Markina, P S Berdonosov, V A Dolgikh, K V Zakharov, E S Kuznetsova, A N Vasiliev

DOI: https://doi.org/10.3367/UFNe.2020.05.038773

Contents

1. **Introduction** **344**
2. **Crystal structure** **345**
3. **Structural phase transition** **347**
4. **Magnetic properties** **348**
5. **Quantum ground state** **350**
6. **Broadband absorption of electromagnetic radiation** **351**
7. **Multiferroic properties of $Cu_3Bi(SeO_3)_2O_2Cl$** **351**
8. **Rare-earth francisites** **353**
9. **Conclusion** **355**

References **356**

Abstract. The synthesis of new geometrically frustrated layered systems has fueled experimental work and progress in building models of low-dimensional magnetism. Compounds with the structure of the francisite mineral, $Cu_3Bi(SeO_3)_2O_2Cl$, are quasi-two-dimensional antiferromagnets with a kagome-type lattice. With the dominant ferromagnetic interaction in the layer and a weak interlayer antiferromagnetic bond, the main noncollinear state of francisite is easily destroyed by an external magnetic field, which opens the possibility of reversible switching between states with the minimum and maximum possible magnetization. In the region of metamagnetic transition, multiferroelectric effects and broadband absorption of electromagnetic waves are observed. The implantation of rare-earth ions *R* into the Bi position is accompanied by spin-reorientation phase transitions in $Cu_3R(SeO_3)_2O_2X$ compounds, where $X = Cl, Br$.

Keywords: francisite, low-dimensional and frustrated magnetism, metamagnetism, multiferroics

1. Introduction

Filling a plane with regular polygons with all lattice vertices topologically equivalent is possible only in eleven ways, known as Archimedean lattices [1]. Virtually each such lattice corresponds to a mineral or artificially created chemical compound. Thus, a triangular lattice corresponds to the lunar mineral hapkeite, Fe_2Si [2], a square lattice is realized in diaboleite $Pb_2Cu(OH)_4Cl_2$ [3], and a honeycomb lattice is implemented in graphene [4]. These are all lattices composed of similar polygons. Among the other eight lattices composed of different regular polygons, the 'bathroom tiles' lattice attracts attention, which is implemented in CaV_4O_9, the first quasi-two-dimensional compound with a spin gap [5]. Spin ladders shifted by a half-period form a 'trellis' ornament in the quasi-two-dimensional compound $Sr_{14-x}Ca_xCu_{24}O_{41+\delta}$, which becomes superconducting under pressure [6]. The Shastry–Sutherland lattice found its implementation in $SrCu_2(BO_3)_2$, where, under the action of a strong magnetic field, a unique sequence of gapped and gapless spin states is realized [7]. The mineral herbertsmithite, the main candidate for detecting the eluding spin fluid, represents the kagome lattice [8]. The compounds described in the present paper belong to this type of Archimedean lattices.

The mineral francisite, $Cu_3Bi(SeO_3)_2O_2Cl$, was found in May 1987 by Glen Francis, a specialist in quality control at the Iron Monarch deposit in South Australia [9]. It immediately caught the attention of experts in mineralogy due to a unique combination of such elements as Cu, Bi, Se, and Cl [10]. It is interesting to physicists, because the magnetoactive copper ions in it form a wavy kagome lattice, and to chemists, because the chlorine ions in the crystal structure channels are not covalently bound to other ions, forming a host–guest system. Subsequent studies have shown that the francisite structure allows a replacement of bismuth with rare–earth elements: selenium with tellurium and chlorine with bromine. As a result, a vast family of isostructure compounds with extremely unusual magnetic properties is formed, in particular, at the expense of the interaction between rare-earth and transition metals. In the present review, specific features of the structure and physical properties of francisite-type compounds are discussed.

M M Markina [(1)], **P S Berdonosov** [(1)], **V A Dolgikh** [(1)], **K V Zakharov** [(1)], **E S Kuznetsova** [(1)], **A N Vasiliev** [(1, 2, 3, a)]
[(1)] Lomonosov Moscow State University, Leninskie gory 1, 119991 Moscow, Russian Federation
[(2)] South Ural State University, prosp. Lenina 76, 454080 Chelyabinsk, Russian Federation
[(3)] National University of Science and Technology MISIS, Leninskii prosp. 4, 119049 Moscow, Russian Federation
E-mail: [(a)] vasil@lt.phys.msu.ru

Received 17 March 2020, revised 4 May 2020
Uspekhi Fizicheskikh Nauk **191** (4) 358 – 371 (2021)
Translated by V L Derbov

Table 1. Parameters of a unit cell of compounds with the francisite structure. Space group *Pmmn*, $Z = 2$ at room temperature.

No.	Formula	*a*, Å	*b*, Å	*c*, Å	Reference
1	$Cu_3Bi(SeO_3)_2O_2Cl$	6.3540(4)	9.6350(5)	7.2330(4)	[11]
2	$Cu_3Bi(SeO_3)_2O_2Br$	6.3900(3)	9.6940(4)	7.2870(3)	[11]
3	$Cu_3Bi(SeO_3)_2O_2I$	6.4360(2)	9.7510(4)	7.3770(3)	[11]
4	$Cu_3Y(SeO_3)_2O_2Cl$	6.2991(1)	9.4411(1)	6.9724(1)	[14]
5	$Cu_3La(SeO_3)_2O_2Cl$	6.39407(18)	9.7310(3)	7.1547(2)	[19]
6	$Cu_3Nd(SeO_3)_2O_2Cl$	6.37775(10)	9.62685(16)	7.09341(11)	[15]
7	$Cu_3Sm(SeO_3)_2O_2Cl$	6.34616(4)	9.56090(7)	7.04377(5)	[16]
8	$Cu_3Eu(SeO_3)_2O_2Cl$	6.3384(1)	9.5341(2)	7.0273(1)	[17]
9	$Cu_3Gd(SeO_3)_2O_2Cl$	6.3220(6)	9.501(1)	7.0202(8)	[13]
10	$Cu_3Dy(SeO_3)_2O_2Cl$	6.313(1)	9.465(2)	6.987(2)	[13]
11	$Cu_3Ho(SeO_3)_2O_2Cl$	6.2999(6)	9.440(1)	6.9723(8)	[13]
12	$Cu_3Er(SeO_3)_2O_2Cl$	6.299(1)	9.432(3)	6.967(2)	[20]
13	$Cu_3Yb(SeO_3)_2O_2Cl$	6.28278(3)	9.39486(5)	6.93291(3)	[18]
14	$Cu_3Lu(SeO_3)_2O_2Cl$	6.2681(1)	9.3756(2)	6.9326(1)	[17]
15	$Cu_3La(SeO_3)_2O_2Br$	6.40071(5)	9.75675(7)	7.17800(5)	[19]
16	$Cu_3Nd(SeO_3)_2O_2Br$	6.382(2)	9.698(3)	7.091(2)	[15]
17	$Cu_3Sm(SeO_3)_2O_2Br$	6.348(1)	9.581(2)	7.079(2)	[13]
18	$Cu_3Gd(SeO_3)_2O_2Br$	6.337(1)	9.5515(8)	7.0540(9)	[13]

2. Crystal structure

All compounds with the francisite structure known to date can be produced by solid-phase synthesis. All of them crystallize in rhombic syngony and belong to the *Pmmn* space group [11–21]. Crystallographic characteristics of these compounds are presented in Table 1.

The francisite structure presented in Fig. 1a is an open framework formed by distorted cubes $[BiO_8]$, planar squares $[CuO_4]$, and pyramids $[SeO_3E]$, where E is a lone electron pair of a selenium atom. The copper atoms are localized in two crystallographically independent positions (Cu1, Cu2), as shown in Fig. 1b. The $[Cu1O_4]$ squares are connected by vertices with the formation of copper-oxygen chains along (100), sewn by $[Cu2O_4]$ squares into a corrugated layer parallel to (110), additionally 'strengthened' by trigonal pyramidal $[SeO_3]$ groups. The localization of copper atoms in these layers corresponds to a distorted kagome lattice in the (*ab*) plane, as shown in Fig. 1c. Along the *c* direction, the layers are connected to each other only by the long (more than 2.8 Å) bismuth–oxygen bond. As a result, along the *c*-axis, the Cu–O bonds form hexagonal channels, in which, alongside lone pairs of selenium (and bismuth), halogen atoms are located (Fig. 2a, b). The lone electron pairs of bismuth atoms act as 'chemical scissors', intercalated between the *ab* planes, while halogen atoms find themselves in the centers of hexagonal tunnels (Fig. 2c).

The hexagonal channel cross section size in a bismuth-containing representative is relatively large for chlorine ions ($r = 1.81$ Å [22]), which leads to a noticeable mobility of chlorine ions and their possible displacement inside the channel. Notably, this explains the presence of a structural transition in $Cu_3Bi(SeO_3)_2O_2Cl$ upon a decrease in temperature to 115 K, which is not observed in a bromide (or iodide) counterpart [23]. It is assumed that the thermal compression of the lattice makes the positions of Cl and Cu2 atoms in the *Pmmn* structure energetically unfavorable, giving rise to antiparallel displacements of these atoms in the crystallographic direction *a* that changes the crystal symmetry to a lower [24] and possibly even acentric one [25]. In this case, parameter *c* doubles upon a decrease in the Cu2–Cl distance from 3.20 Å at 150 K to 2.82 Å at 50 K [23]. The bromine ion ($r = 1.96$ Å [22]) has no such freedom, which makes the bromide 'construction' the most stable, while in the case of the iodide analog, the appearance of stress in the structure due to the large value of the iodine ion radius ($r = 2.2$ Å [22]) can be hypothesized. This synthetic analog of francisite can rather be considered a metastable phase. In the literature, the change in $Cu_3Bi(SeO_3)_2O_2Cl$ structure under heating is described [26]. It is shown that, under heating to 500 °C, the structure expands inhomogeneously and the maximal change occurs in the structure parameter *c*, which corresponds to an increase in the distance between the kagome networks and, respectively,

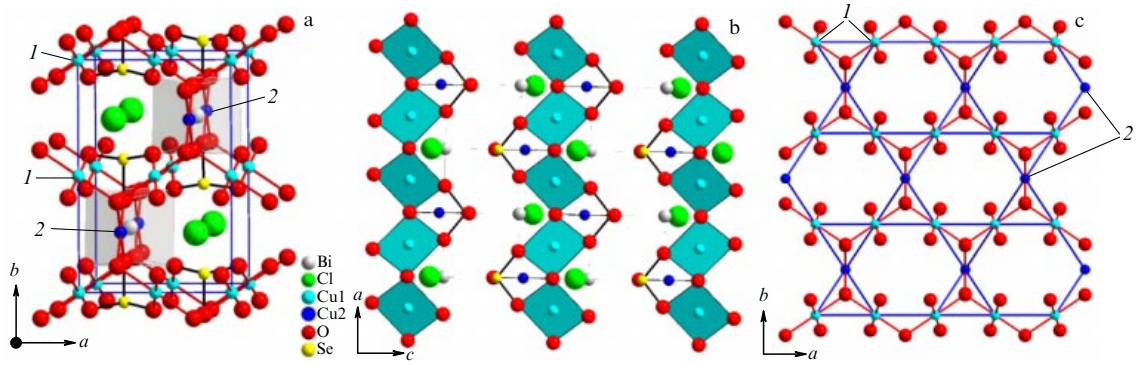

Figure 1. (Color online.) Crystal structure of $Cu_3Bi(SeO_3)_2O_2Cl$: (a) in the representation of chemical bonds (darkening denotes BiO_8 coordination cubes); (b) in the polyhedron representation; (c) kagome lattice of copper atoms in oxygen environment. Cu1 atoms are shown in blue (*1*) and Cu2 atoms, in dark blue (*2*).

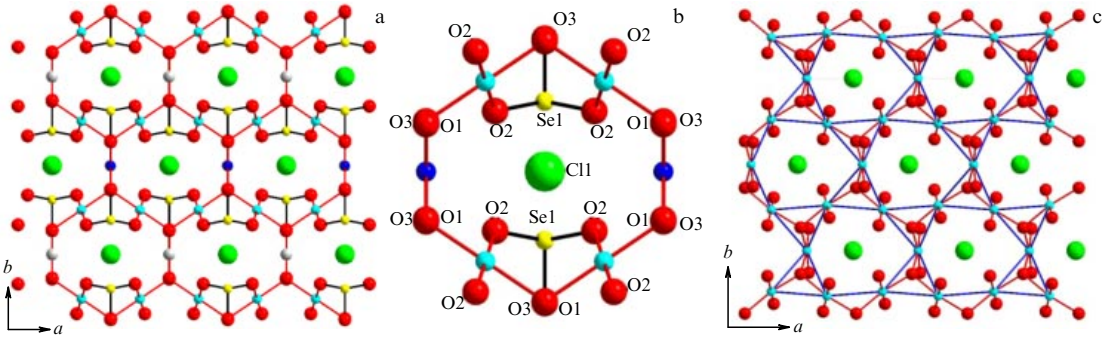

Figure 2. (Color online.) Hexagonal channels in the $Cu_3Bi(SeO_3)_2O_2Cl$ structure, formed by Cu–O bonds. (a) Projection on the *ab* plane; (b) configuration of an individual hexagon; (c) kagome lattice distortion in the $Cu_3Bi(TeO_3)_2O_2Cl$ structure [12].

between Bi–Se–Cu–O layers in the structure. Based on the above regularities, it can be believed that the instability of $Cu_3Bi(SeO_3)_2O_2I$ [11] and the impossibility of obtaining iodide analogs with the composition $Cu_3M(SeO_3)_2O_2I$ (M = Y, La, Pr, Nd, Sm, Eu, Gd, Tb, Dy, Ho, Er, Tm, Yb, Lu) [13] is due to the dimensional factor. This is clearly manifested in the partial replacement of selenium ions with larger tellurium ions in the system $Cu_3Bi(Se_{1-x}Te_xO_3)_2O_2Cl$ [27, 28], where the formation of solid solutions with *Pmmn* symmetry is observed only in the composition interval $0 \leqslant x \leqslant 0.6$ (Table 2).

The substitution of tellurium in the selenium position in the *ab* plane increases lattice parameters *a* and *b* but decreases parameter *c*, although the difference in *c* values for samples of compositions with $x = 0$ and 0.2 is below the resolution power of high-resolution synchrotron X-ray diffraction (with an angular step of 0.004°) used in Ref. [27]. The Cu1 – O1 – Cu1 bond angle decreases by nearly 0.83% and the Cu1 – O1 – Cu2 angle increases by 1.6% with such a replacement. However, the bond lengths for Cu1 – O1 – Cu1 and Cu1 – O1 – Cu2 in this case increase by 0.66 and 1.73%, respectively [27]. As mentioned above, the $Cu_3Bi(Se_{1-x}Te_xO_3)_2O_2Cl$ solid solutions exist in a limited concentration interval (up to $x = 0.6$). Nevertheless, a tellurium-containing phase $Cu_3Bi(TeO_3)_2O_2Cl$ isostoichiometric to francisite exists [12], but is not isostructural to it. It crystallizes in the space group *Pcmn* with the unit cell parameters $a = 6.3179$, $b = 9.8524$, $c = 14.358$ Å, $Z = 4$. The general algorithm of this phase construction is like that of francisite, where two crystallographically nonequivalent copper atoms with planar coordination by four oxygen atoms are present. Oxide squares connected by vertices form a layer in which copper ions make a kagome lattice. The minimum interatomic distance Cu2–Cl (2.718 Å) in this compound is smaller than the corresponding distance in francisite; therefore, according to the valence sum rule, a coordination polyhedron for this copper atom is the square pyramid $Cu2O_4Cl$ [12]. The bismuth atom still has a distorted cubic coordination, and the tellurium atom, similar to the selenium atom in francisite, is characterized by a single-sided triple oxygen coordination, complemented by a lone electron pair (E) with the formation of a TeO_3E group. The larger tellurium ion size causes an increase in the distance E–Cl in $Cu_3Bi(TeO_3)_2O_2Cl$ relative to that observed in the selenium counterpart, which leads to a repulsion of the chlorine ion lone electron pair from the tellurium atom, due to which in the tellurium-containing phase a wider range of Cu–Cl bond lengths is formed. Also, the Te–O bonds are somewhat longer (by nearly 0.2 Å) than Se–O distances, which makes oxygen ions move from the high-symmetry positions, giving rise to an additional oxygen position and setting the copper atoms in motion. These circumstances lead to doubling of the parameter *c* and to distortion of the kagome lattice of copper atoms in the structure, as shown in Fig. 2c. Upon replacement of the chloride anion with bromide, in the phase structure of the composition $Cu_3Bi(SeO_3)_2O_2Cl_{0.5}Br_{0.5}$, averaging of unit cell parameters of the phase compared to pure chloride or bromide is observed (Table 1, 2) [27, 28].

In the family of rare-earth francisites, a tendency toward a decrease in Cu1–Cu1 and Cu1–Cu2 bond lengths is distinctly manifested upon proceeding along the lanthanides row; however, there are no explicitly expressed tendencies toward changes in Cu1–Cu2–Cu1 angles. This must lead to the narrowing of hexagonal channels in the structures of this row, which may be related to the observed termination of the bromide family, extending from La to Gd, and the absence of analogous compounds with iodine. The unit cell parameters in francisites containing different halogens change in an expected way, but the growth in *a*, *b*, and *c* upon a transition from chlorides to iodides is not uniform: the change in parameter *c* is maximum (in the bismuth representative by 42%) due to a greater mobility of kagome lattices than halogen atoms inside the lattices. At the same time, the Se–O distances in this subfamily are practically unchanged.

As noted in paper [29] devoted to cation inorganic materials that can be used to detect and analyze anion

Table 2. Crystallographic characteristics of francisite-like phases of $Cu_3Bi(TeO_3)_2O_2Cl$, space group *Pcmn*, $Z = 4$, as well as $Cu_3Bi(Se_{1-x}Te_xO_3)_2O_2Cl$ and $Cu_3Bi(SeO_3)_2O_2Cl_{0.5}Br_{0.5}$, space group *Pmmn*, $Z = 2$.

No.	Composition	*a*, Å	*b*, Å	*c*, Å	Reference
1	$Cu_3Bi(TeO_3)_2O_2Cl$	6.3719(8)	9.8524(12)	14.358(2)	[12]
2	$Cu_3Bi(Se_{0.8}Te_{0.2}O_3)_2O_2Cl$	6.228352(19)	9.5232(35)	7.13953(22)	[22]
3	$Cu_3Bi(Se_{0.6}Te_{0.4}O_3)_2O_2Cl$	6.30374(10)	9.57760(17)	7.13238(11)	[11]
4	$Cu_3Bi(Se_{0.4}Te_{0.6}O_3)_2O_2Cl$	6.31166(10)	9.60912(17)	7.12366(12)	[12]
5	$Cu_3Bi(SeO_3)_2O_2Cl_{0.5}Br_{0.5}$	6.27115(8)	9.52133(14)	7.15295(10)	[10]

contamination, an increase in the mobility of halogen ions in the channels of the francisite crystal structure would give rise to an implementation of electrolytic cells on mobile positively charged ions.

3. Structural phase transition

The study of the optical characteristics of francisites led to the discovery of a structural phase transition in compounds with chlorine at a temperature of ~ 115 K [30]. Below this temperature, 16 additional modes appeared in the phonon spectrum; moreover, with a decrease in temperature, a sharpening of many modes was observed. In addition to new phonons, softening of the low-frequency mode (at 5 K to $\sim 30\%$ of the value at 300 K) along direction b was found, which is characteristic of displacement-type ferroelectrics. It was impossible to determine the symmetry group exactly, since both $P2_1mn$ (polar) and $Pcmn$ (nonpolar) groups generally corresponded to changes in the phonon modes.

The appearance of new low-temperature reflexes in the high-resolution spectra of synchrotron diffraction [26] and anomalies in specific heat and permittivity of $Cu_3Bi(SeO_3)_2O_2Cl$ became direct confirmation of a second-order structural phase transition at 115 K. Note that, as shown in Fig. 3, no structural phase transition is observed in the compound with bromine, although a magnetic phase transition is observed in the same temperature interval, as in a chlorine-containing compound. The permittivity anomaly in $Cu_3Bi(SeO_3)_2O_2Cl$ at $T_S = 115$ K is not great ($\Delta\varepsilon/\varepsilon \sim 2\%$), and the anomaly itself has a wide temperature range. A blurred loop of polarization $P(E)$ was also found that manifests itself at $T < T_S$; however, the loop shape does not correspond to expectations for an antiferroelectric and rather testifies to the presence of small polar phase inclusions in the sample studied [27].

Using the methods of structural analysis, the authors of Ref. [26] confirmed that at $T > 200$ K the crystal symmetry group of $Cu_3Bi(SeO_3)_2O_2X$ (X = Br, Cl) corresponds to space group $Pmmn$. At $T < T_S = 115$ K in the $Cu_3Bi(SeO_3)_2O_2Cl$ lattice, a superstructure with period doubling along the c-axis is formed: $a \times b \times 2c$ (Fig. 4). The lattice period doubling made it possible to describe the appearance of 16 additional phonon modes, found in Ref. [30], without using the polar group $P2_1mn$. Distinct low-temperature reflexes correspond to $Pcmn$ symmetry with antiparallel displacements of Cl and Cu2 ions along the a-axis. It was also noted in [26] that even at $T > T_S$ the $Cu_3Bi(SeO_3)_2O_2Cl$ crystal structure is better described in the framework of the distorted $Pcmn$ model than in the framework of the more symmetric $Pmmn$ model. Such behavior is observed in ferroelectrics and antiferroelectrics, where dipoles are formed at temperatures above the temperature of a transition to the ordered state.

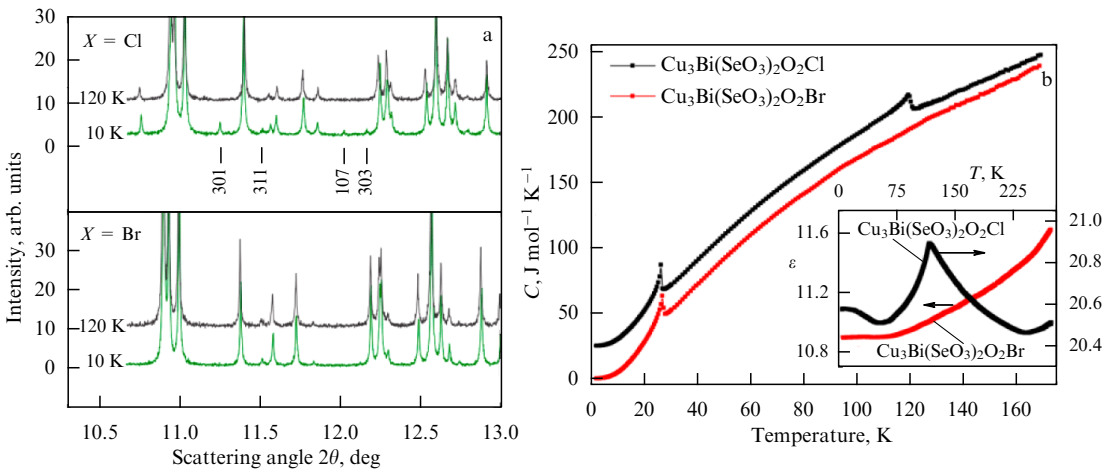

Figure 3. (a) Diffraction patterns of $Cu_3Bi(SeO_3)_2O_2X$ (X = Cl, Br) compounds [26]; (b) temperature dependences of specific heat of these compounds (inset shows temperature dependences of permittivity) [27].

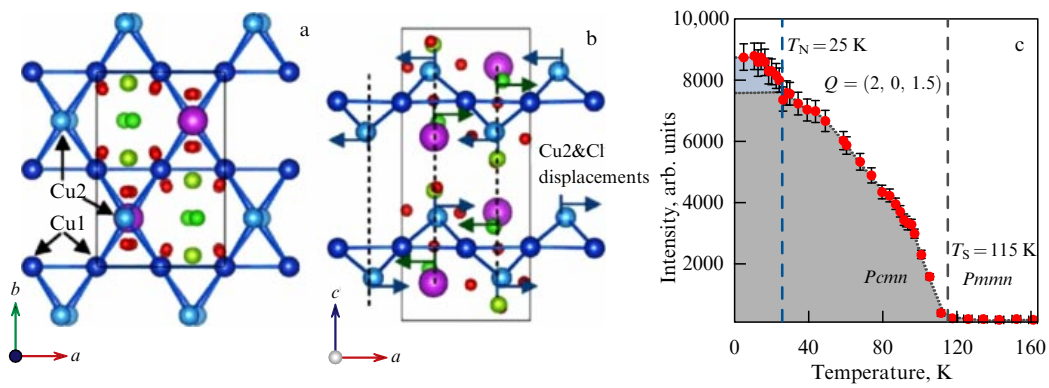

Figure 4. (a, b) Collective displacements of Cu1 and Cu2 in the low-temperature phase of $Cu_3Bi(SeO_3)_2O_2Cl$; (c) temperature dependence of reflex intensity $Q = (2, 0, 1.5)$ [28].

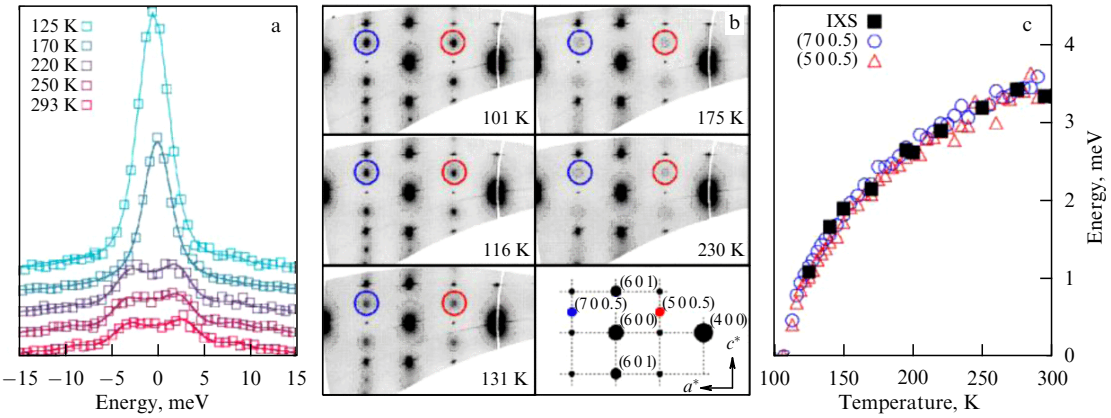

Figure 5. (a) Evolution of spectrum of X-ray inelastic scattering from room temperature to T_S; (b) reconstructed ($h0l$) layer of $Cu_3Bi(SeO_3)_2O_2Cl$ in the reciprocal space at several temperatures; (c) evolution of soft mode energy with temperature (IXS denotes inelastic X-ray scattering) [22].

Detailed studies of neutron diffraction and inelastic scattering of neutrons by a $Cu_3Bi(SeO_3)_2O_2Cl$ single crystal confirmed the *Pcmn* symmetry of the low-temperature phase and the character of collective displacements of Cl and Cu2 [28]. It was established that these displacements occur from the position $x/a = 1/4$ at $T > T_S$ to the position $x/a = 1/4 + \Delta_{Cu2,Cl}$ below T_S, where $\Delta_{Cu2} = 0.026$ and $\Delta_{Cl} = 0.031$ at 50 K. As a result of such displacement, the Cl–Cu2 bond in the low-temperature phase of $Cu_3Bi(SeO_3)_2O_2Cl$ becomes shorter. In $Cu_3Bi(SeO_3)_2O_2Br$, displacements of Br and Cu2 ions also take place, but there is no clearly expressed low-temperature phase in which these displacements would be ordered. In $Cu_3Bi(SeO_3)_2O_2I$, no displacement of ions was detected. Recently, using the inelastic scattering of X-rays and thermodiffusion scattering, a soft phonon mode was found in the interval $T > 115$ K [22]. As shown in Fig. 5, at high temperatures in the high-symmetry phase, the soft mode is observed at the Brillouin zone boundary at (0, 0, 0.5). In the low-symmetry phase, as a result of unit cell doubling, this soft mode moves to the Brillouin zone center and is a totally symmetric mode, which could be fixed in Raman spectra.

According to the theory of antiferroelectric phase transitions [23], antiferroelectrics undergo a structural transition from a high-symmetry phase to a low-symmetry one, in which electric dipoles arise or become ordered. These dipoles form lattices of opposite polarizations, which macroscopically cancel each other. By analogy with ferroelectrics, antiferroelectric transitions can be classified following two idealized models: an order–disorder transition and a displacement-type transition. Conceptually, the displacement-type antiferroelectric transition should be initiated by an antipolar soft phonon mode, i.e., a structural instability at the Brillouin zone boundary. Such a mode implies only antiparallel displacements of ions, directly coupled via the phonon branch with the polar mode in the zone center, caused by synphase motions of the same ions. Upon a decrease in temperature, the frequency of the antipolar phonon decreases, and the ion displacements ultimately become frozen at T_S, reducing the symmetry in the antiferroelectric structure, where the polar instability manifests itself under the action of an electric field. Phenomenologically, antiferroelectric transitions of the first and second order are distinguished as transitions between two nonpolar phases, accompanied by a jump-like permittivity anomaly. In the low-symmetry phase, the application of an electric field leads to

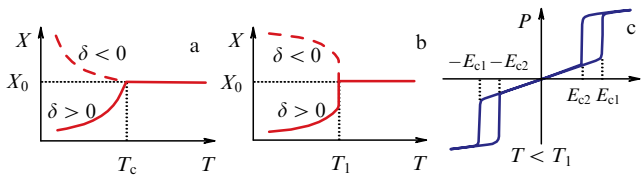

Figure 6. (a, b) Theoretical dependences of permittivity for antiferroelectric transition of the second (a) and first order (b); (c) double hysteresis loop $P(E)$ accompanying the transition from antiferroelectric to ferroelectric phase [23].

a phase transition to a polar phase (ferri- or ferroelectric), which yields a characteristic double hysteresis loop in the dependence $P(E)$ (Fig. 6).

For real substances, there is still no criterion to define antiferroelectric crystalline structure and no consensus about a rigorous definition of antiferroelectric transitions. In classical paper [24], Kittel describes a model of an elementary antiferroelectric crystal, which to date has not found experimental implementation. The authors of Ref. [23], based on experimental studies and calculations using the density functional theory, make a conclusion that the transition at $T_S = 115$ K in $Cu_3Bi(SeO_3)_2O_2Cl$ is a rare type of antipolar transition caused by a soft phonon mode. The observed transition most closely corresponds to an elementary transition in the Kittel model.

4. Magnetic properties

The investigation of the physical properties of francisite synthetic analogs began from the development of hydrothermal synthesis of $Cu_3Er(SeO_3)_2O_2Cl$ and establishing its crystal structure at room temperature [20]. Only after this were single crystals of synthetic $Cu_3Bi(SeO_3)_2O_2Cl$ obtained for the first time using the method of chemical transport and the temperature dependences of crystal lattice parameters in the temperature interval 273–743 K [21]. Later, using solid phase synthesis, halogen-substituted compounds $Cu_3Bi(SeO_3)_2O_2X$, where X = Cl, Br, I [11], were obtained, and their crystal structure was specified. It was established that copper layers in the *ab* plane have a distorted kagome structure with two nonequivalent positions of Cu^{2+} ions. In Ref. [11], the magnetic properties of francisites with Cl and Br were also investigated in a wide range of temperatures. As

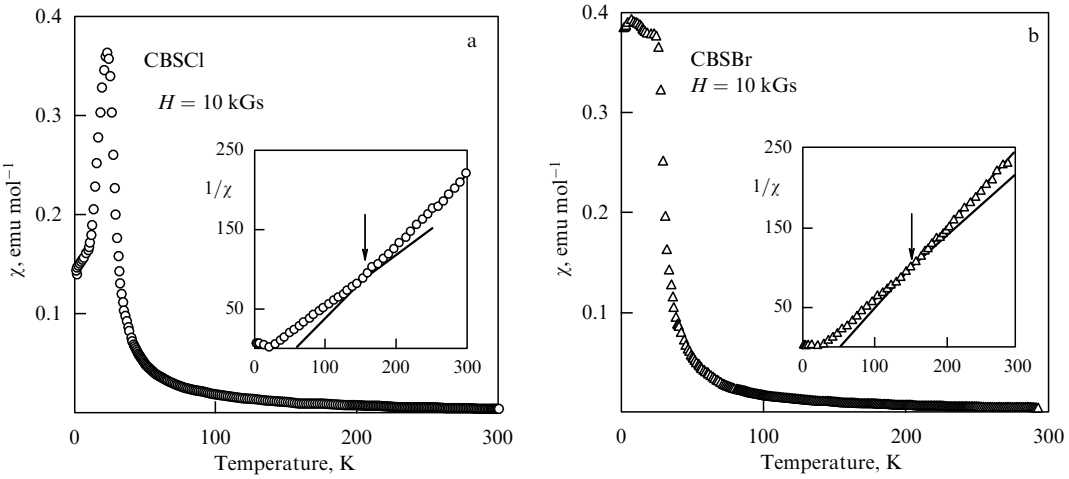

Figure 7. Temperature dependences of magnetic susceptibility in $Cu_3Bi(SeO_3)_2O_2Cl$ (a) and $Cu_3Bi(SeO_3)_2O_2Br$ (b) [11]. The insets show the dependences of inverse magnetic susceptibility in these samples.

shown in Fig. 7, at low temperatures, the formation of long-range magnetic order was found at the Néel temperatures of 23.5 and 24.2 K for $X = \mathrm{Cl}$ and Br, respectively. Moreover, it turns out that the temperature dependences of magnetic susceptibility at $T < T^* \sim 150$ K and $T > T^*$ are described by the Curie–Weiss laws with different sets of parameters. In particular, at $T > T^*$, the Weiss temperature Θ, determined by the scale of exchange interactions, is nearly two times greater than the value of Θ at $T < T^*$. Upon a transition from low to high temperatures, the value of Curie constant C related to the magnitude of the effective magnetic moment in a substance also considerably decreases. This is most likely because, at low temperatures comparable by order of magnitude with the basic parameters of the exchange interaction, the description of experimental data by the Curie–Weiss law is incorrect.

The burst of interest in synthetic analogs of francisite is related to the appearance of a number of experimental papers, in which the structural and magnetic transformations in these substances were discussed. In two papers of this series, evidence of an anisotropic metamagnetic transition in $Cu_3Bi(SeO_3)_2O_2Br$ [31] and $Cu_3Bi(SeO_3)_2O_2Cl$ [30] was published. In the field dependences of magnetization $M(B)$ of single crystals of these compounds in the ordered state ($T < T_N$), striking anomalies in the form of jumps and a hysteresis loop along different axes were observed. In a weak magnetic field of $B_C \sim 0.8$ T applied along the c-axis in compounds with chlorine and bromine, a metamagnetic phase transition from the antiferromagnetic to ferromagnetic phase was observed. The anisotropy also manifested itself in the temperature dependences of magnetic susceptibility (Fig. 8).

Metamagnets are magnetically ordered materials that undergo phase transitions from a state with low magnetization (commonly, an antiferromagnetic state) to a state with high magnetization (commonly, a ferromagnetic state) induced by a magnetic field. Due to demagnetizing fields, transitions from one state to another turn out to be extended

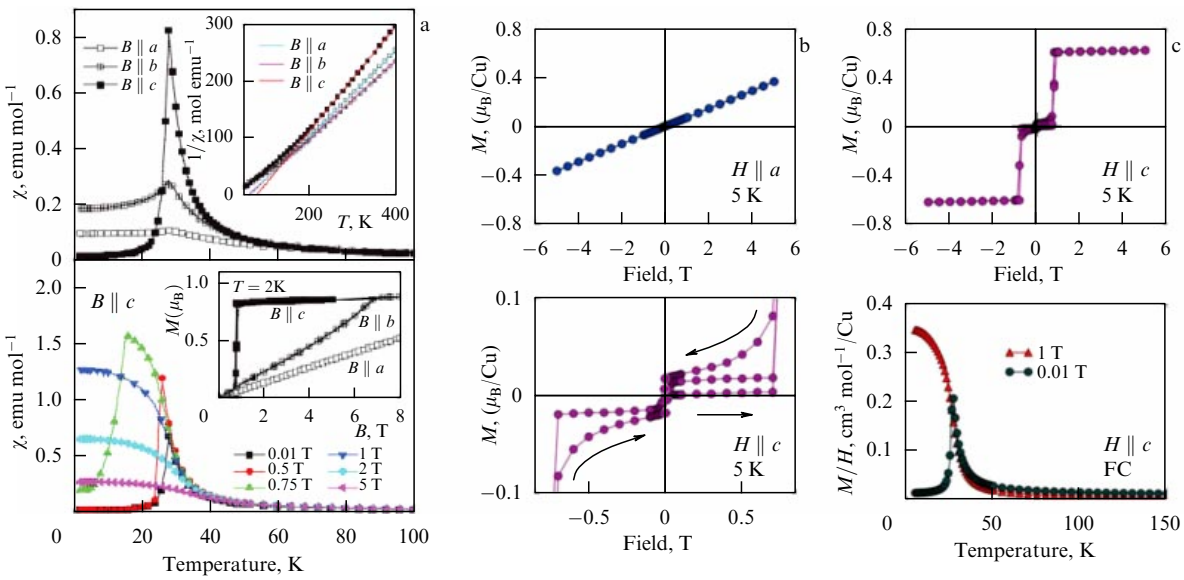

Figure 8. (a) Temperature and field dependences of magnetization in $Cu_3Bi(SeO_3)_2O_2Br$ [31]. (b, c) Temperature and field dependences of magnetization in $Cu_3Bi(SeO_3)_2O_2Cl$; μ_B is the Bohr magneton [30].

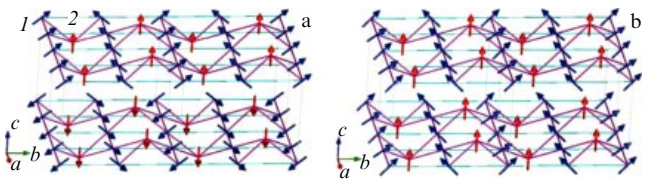

Figure 9. (Color online.) Magnetic structure of $Cu_3Bi(SeO_3)_2O_2Br$ (a) in the absence of a magnetic field, (b) in a magnetic field of $B_C = 1$ T. Magnetic moments on ions in Cu1 position are shown by blue tilted arrows (*1*), in Cu2 position by red vertical arrows (*2*) [31].

over the magnetic field. In the corresponding intermediate region, domains of antiferromagnetic and ferromagnetic phases coexist. Thanks to multiple possible configurations of these domains, a wide virtually continuous spectrum of magnetic excitations is implemented. The most studied mechanism in this area is, apparently, the band metamagnetism observed under a jump-like transition of the paramagnetic system of band electrons to a magnetically ordered state under the action of a magnetic field [25]. This phenomenon was experimentally observed in some intermetallic compounds; in particular, in Refs [32, 33] a metamagnetic transition from an antiferromagnetic to a ferromagnetic state was described.

Based on the results of neutronographic measurements, it was found that at low temperatures in $Cu_3Bi(SeO_3)_2O_2Br$ a noncollinear six-sublattice antiferromagnetic structure is realized, shown in Fig. 9 [31]. This structure can be presented as a sequence of antiferromagnetically coupled three-sublattice ferromagnetic layers. The canting angle of magnetic moments in Cu1 amounts to $\sim 52^\circ$ from axis c to axis b. The moments in Cu2 ions are oriented parallel to axis c. Under the action of an external magnetic field B_C with an induction of less than 1 T directed along axis c, a flip of each second layer occurs in the positive direction of axis c. Noticeably greater fields are required to bring the copper magnetic moments to axes a and b. This flip is exactly a metamagnetic transformation of the first order.

The interest shown by research teams dealing with *ab initio* calculations of exchange integrals in new objects with the kagome-type magnetic structure was so great that such calculations for francisites were performed before the confirmation of a structural transition in $Cu_3Bi(SeO_3)_2O_2Cl$. The Hamiltonian of the problem and the results of calculations were corrected several times in a series of papers [26, 28, 34, 35] before it was possible to describe both the ground state and all the experimentally observed phenomena, including the substitution of one halogen with another. We recall that in the case of predominating antiferromagnetic interactions, the ground state of a kagome lattice with Heisenberg ions with the spin $S = 1/2$ is a spin liquid. Strong spin-spin correlations are characteristic of this state, but it does not reach a long-range magnetic order. The most well-known example of realizing such a state is the mineral herbertsmithite, $ZnCu_3(OH)_6Cl_2$ [36, 37], where, in spite of the presence of strong antiferromagnetic interaction ($\Theta \sim 300$ K), no long-range order is established down to 50 mK. In synthetic analogs of francisite $Cu_3Bi(SeO_3)_2O_2X$, where $X = $ Cl, Br, on the contrary, the magnitude of the paramagnetic Weiss temperature is not high, ~ 50 K, and corresponds to ferromagnetic interaction, while the long-range order is established at ~ 24 K.

The formation of a noncollinear magnetic structure indicates the presence of a competition between magnetic interactions, as well as the necessity to consider the Dzyaloshinskii–Moriya interaction between Cu1 and Cu2, which stabilizes the ground state. Basic magnetic interactions in francisites were estimated in Ref. [34] using the density functional theory for space symmetry group *Pmmn*. It was found that isotropic interactions of the nearest neighbors (J_1) between Cu1 spins along axis a, and J_1' between Cu1 and Cu2 spins along diagonal a–b are mainly ferromagnetic. A relatively strong interaction of next to nearest neighbors between Cu1 spins along axis b (J_2) is antiferromagnetic and is a source of frustration. It is also necessary to take into account the weak interlayer (along c) antiferromagnetic interactions $J_{\perp 1}$ and $J_{\perp 2}$ between Cu1 and Cu2 ions. To stabilize the ground state, the Hamiltonian of the problem was complemented with antisymmetric anisotropic Dzyaloshinskii–Moriya interaction between Cu1 and Cu2 spins with the dominating component of interaction vector D_a along axis a, the sign of which alternates along axis b. Other components of the vector were chosen as $D_b \approx D_c \approx D_a/3$. The asymmetric part of anisotropic exchange interaction was also considered using second-order tensors; however, its role was found to be unessential. Modeling of metamagnetic behavior in $Cu_3Bi(SeO_3)_2O_2Br$ along three crystallographic directions was carried out in Ref. [35] using the mean-field Hartree–Fock solution of the Hubbard model. A unique feature of francisites is associated with the metamagnetic transition, namely, the broad-band absorption of electromagnetic radiation.

5. Quantum ground state

The refined symmetry of the low-temperature phase required updating and specifying the Hamiltonian of the problem, the noncollinear magnetic structure of the ground state, and the signs and magnitudes of exchange integrals that determine it. It was established that the magnetic structure of $Cu_3Bi(SeO_3)_2O_2Cl$ in the ground state is similar to the earlier determined structure of $Cu_3Bi(SeO_3)_2O_2Br$, but with greater canting (by 59°) of magnetic moments of Cu1 ions from axis c to axis b [28]. An adequate description of the results of neutron experiments in $Cu_3Bi(SeO_3)_2O_2Cl$ has been achieved with the following set of parameters in the Hamiltonian

$$H_0 = J_1 \sum_{i=1,3;\, j=2,4} \mathbf{S}_i\mathbf{S}_j + J_1' \sum_{i=1-4;\, j=5} \mathbf{S}_i\mathbf{S}_j + J_2 \sum_{i=1,2;\, j=3,4} \mathbf{S}_i\mathbf{S}_j$$

$$+ J_{\perp 1} \sum_{i=1-4;\, j=6} \mathbf{S}_i\mathbf{S}_j + J_{\perp 2} \sum_{i=5;\, j=6} \mathbf{S}_i\mathbf{S}_j + \mathbf{D} \sum_{i=1-4;\, j=5} \mathbf{S}_i \times \mathbf{S}_j$$

(the quantities are in meV): three exchange integrals inside the layer are $J_1 = -6.6(3)$, $J_1' = -5.8(5)$, $J_2 = 5.7(3)$, two interlayer exchange integrals are $J_{\perp 1} = -0.04(4)$, $J_{\perp 2} = 0.02(2)$, and the components of the Dzyaloshinskii–Moriya interaction vector are $D_a = 1.3(1)$, $D_b = D_c = D_a/10$. Moreover, it also appeared to be necessary to take into account the second-order tensors $\Gamma_{1,2}$, $\Gamma_{5,2}$, and $\Gamma_{3,2}$ describing symmetric anisotropic modifications of the exchange interaction H_{AE}, arising due to the spin-orbit interaction,

$$H_{AE} = \mathbf{S}_i \Gamma_{i,j} \mathbf{S}_j \,.$$

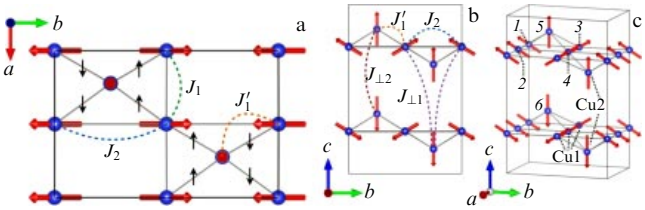

Figure 10. Refined magnetic structure of $Cu_3Bi(SeO_3)_2O_2Cl$ [28]. (a) Orientation of spins in *ab*-plane, (b) spin orientation in *bc*-plane, (c) arrangement of spins in a 3D representation.

Note that, in the ground state structure calculations for francisite with bromine, the calculated interactions H_{AE} turned out to be negligibly small (Fig. 10).

6. Broadband absorption of electromagnetic radiation

The determination of mechanisms responsible for broadband absorption of electromagnetic radiation, controlled by an external field, became an interesting problem that arose in studies of metamagnetic transformations in low-dimensional and frustrated magnets with the structure of francisite. This is a fundamental scientific problem, many aspects of which (in particular, multiferroelectric behavior) are only beginning to manifest themselves. However, the scope of the problem is far beyond the framework of academic study. This is a case where a complex physical phenomenon not observed earlier has clear prospects of practical use. Processing microwave and optical signals using francisite-based elements will be possible only at low temperatures (below 24 K), but this factor only facilitates the improvement of the signal-to-noise ratio in electronic systems. Actually, the technique for dealing with metamagnetic materials is the same as presently used for operating with superconducting bolometers. However, to regulate the absorption (transmission) of electromagnetic radiation, moderately strong ($B \sim 1$ T) magnetic fields will be necessary. Such fields are created either by electromagnets or by stationary Halbach systems.

The phenomenon of broadband absorption of electromagnetic waves was experimentally observed in quasi-two-dimensional metamagnetic $Cu_3Bi(SeO_3)_2O_2Br$ [30, 38–40]. The range of broadband absorption spanned at least ten decades in frequency, from a few hundred Hz to a few hundred GHz. Of particular importance is that, in a mixed state of francisite, it is possible to control the absorption by an external magnetic field. The broadband absorption of electromagnetic radiation is highly in demand in modern electronics. Applications of this effect include radiofrequency/optical filtering, processing of optical signals, and electromagnetic screening. The main drawback of materials used at present is the relatively narrow range of absorption, spanning only a few decades in frequency. Moreover, the absorption in these materials is not controllable by external factors. In this connection, the controllable broadband absorption of electromagnetic radiation in metamagnets seems to be an extremely useful effect revealing new functional properties of these objects.

From the point of view of research and the application of broadband absorption of electromagnetic waves, both polycrystals and single crystals of francisites are of interest. Absorption bands are noticeably broader in polycrystals; however, monocrystals allow 'cutting' definite windows in a given range of frequencies. The main result of these studies is presented in Fig. 11a. It is seen that, independent of frequency in the GHz range, in a certain interval of magnetic field magnitudes a strong nonresonant absorption of electromagnetic radiation occurs in $Cu_3Bi(SeO_3)_2O_2Br$. It is exactly this interval where antiferromagnetically and ferromagnetically ordered domains coexist, as shown in Fig. 11c, d. The region of metamagnetic transformation existence is limited by the temperature of long-range magnetic order formation. This temperature amounts to 24 K in the classical francisite and reaches 40 K in rare-earth francisites.

7. Multiferroic properties of $Cu_3Bi(SeO_3)_2O_2Cl$

In a recent paper on the investigation of the physical properties of francisite [41], it was shown that this material is a dielectric with polarization induced by a magnetic field,

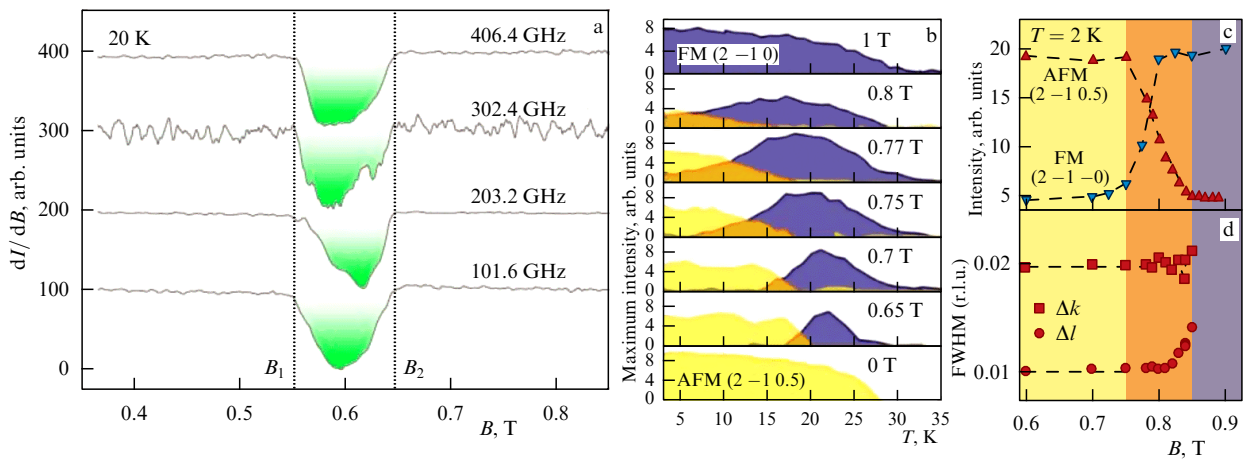

Figure 11. (Color online.) (a) Set of nonresonant absorption spectra at 20 K and at various frequencies. Vertical shift of each spectrum corresponds to the frequency. Vertical lines show the lower, B_1, and upper, B_2, critical fields, corresponding to the boundaries of the strongly absorbing mixed phase in $Cu_3Bi(SeO_3)_2O_2Br$ [40]. (b) Temperature dependences of ferromagnetic (FM, blue) and antiferromagnetic (AFM, yellow) reflections in neutron diffraction, corresponding to the high- and low-field phases, respectively, measured in a magnetic field applied along the *c*-axis. Field dependences of intensity (c) and width of the antiferromagnetic peak (d) at 2 K [39]. The latter do not change (they are limited by the instrumental resolution), since the peak virtually vanishes. This means that both types of ordering are strongly correlated in the mixed phase of $Cu_3Bi(SeO_3)_2O_2Br$.

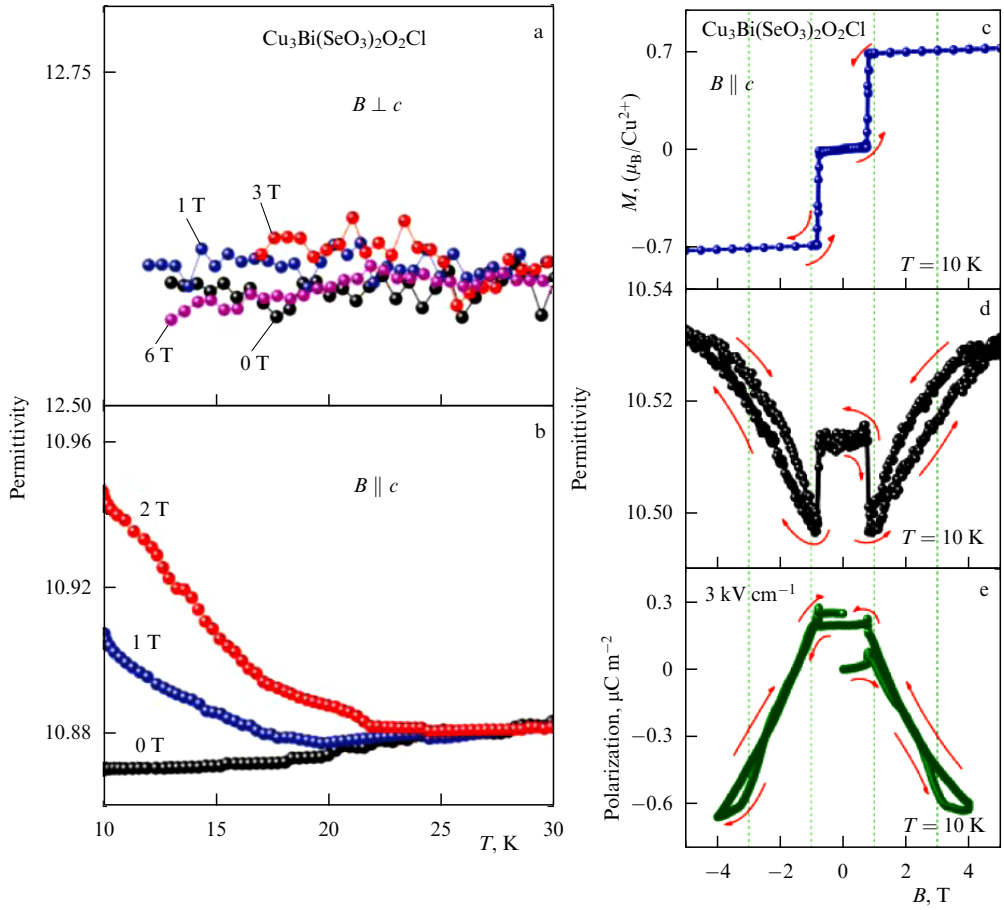

Figure 12. Temperature dependences of $Cu_3Bi(SeO_3)_2O_2Cl$ permittivity in a magnetic field, perpendicular (a) and parallel (b) to the *c*-axis. Field dependences of magnetization (c), permittivity (d), and polarization (e) at 10 K.

i.e., a multiferroic. In Ref. [27], an anomaly of permittivity at T_S was found; however, at T_N, no anomalies were observed. It turned out that the anomaly at T_N manifests itself upon the application of a magnetic field in a certain direction. In the temperature dependence of specific heat, the sharp peak at T_N is preserved only in magnetic fields $B < B_C$, while in stronger fields the peak turns into a strongly blurred anomaly, shifted towards higher temperatures. In the temperature dependence $\varepsilon(T)$, an anisotropic behavior is observed: at $B = 0$ there is no anomaly; in fields $B \perp c$ no anomaly is observed; but in the case of $B \parallel c$ at $B > B_C$ and $T < T_N$, a sharp increase in the permittivity occurs, resembling the model antiferroelectric transition of the second order described in Ref. [23].

To establish a relation between magnetism and electric properties, in Ref. [41] the field dependences of magnetization, permittivity, and polarization were investigated at the same temperature below T_N in a field directed along the *c*-axis. Upon the metamagnetic transition, the curve $M(B)$ demonstrates a step, related to a flip of magnetic moments in each second layer (*ab*) and the transition to a ferromagnetic state with high magnetization. In fields $B < B_C$, the value of ε is constant, upon reaching the value B_C the dependence $\varepsilon(B)$ has a discontinuity with a jump down, and upon a further increase in the field, $\varepsilon(B)$ grows and a hysteresis is observed when increasing and decreasing the magnetic field at $B > B_C$. The magnitude of the polarization vector is not sensitive to the magnetic field at $B < B_C$ either, and upon reaching B_C a peak of polarization appears, while in the region $B > B_C$ a decrease in $P(B)$ takes place, accompanied by a hysteresis

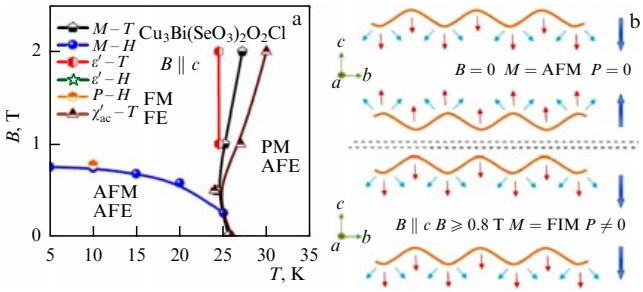

Figure 13. (a) Magnetic phase diagram of $Cu_3Bi(SeO_3)_2O_2Cl$ in a field parallel to the *c*-axis. (b) Schematic diagram of reorientation of magnetization and polarization vectors during a metamagnetic phase transition [41].

when increasing and decreasing the field. The hysteresis may be due to the high inertia of electric dipoles compared to magnetic spins (Fig. 12).

As a result of detailed investigations of magnetization, specific heat, and polarization of the $Cu_3Bi(SeO_3)_2O_2Cl$ single crystal in the fields $B \parallel c$ and $B \perp c$, a magnetic phase diagram was drawn up (Fig. 13) [41]. It was ascertained that the spin-flip transition induced by the magnetic field brings the electric subsystem from the antiferroelectric to the ferrielectric state. Thus, the francisite can be considered a type-II multiferroic, analogous to $DyFeO_3$, in which the reorientation of Fe magnetic moments under the action of an external field creates an exchange striction between the layers of Dy and Fe leading to ferroelectric ordering [42].

Table 3. Parameters of $Cu_3R(SeO_3)_2O_2Cl$ (R = Y, La, Eu, Lu) magnetic system.

$Cu_3R(SeO_3)_2O_2Cl$	Y [14]	La [19]	Eu [17]	Lu [17]
C, emu mol^{-1} K^{-1}	1.23	1.35	1.5	1.6
Θ, K	75	52.9	69	64
$\mu_{\text{eff}}^{\text{exp}}$ (μ_B)	3.1	3.3	3.5	3.5
$\mu_{\text{eff}}^{\text{theor}}$ (μ_B)	3.4	3.4	3.4	3.4
χ_0, emu mol^{-1}	-1.56×10^{-4}	-5.0×10^{-4}	-1.8×10^{-4}	-1.8×10^{-4}
T_N, K	35	31.2	36	38
B_C, T	2.6	2.4	2.6	2.9

8. Rare-earth francisites

The rare-earth francisite $Cu_3Er(SeO_3)_2O_2Cl$ was first obtained and described in Ref. [20]. In Ref. [13], the compounds $Cu_3R(SeO_3)_2O_2X$ (R = La, Nd, Sm, Eu, Gd, Dy, Ho, Er, Yb; X = Cl, Br) were synthesized. Oxochlorides of this composition exist with all rare-earth elements, while the oxobromides exist only with R = La–Gd because of the dimensional factor. The variation in the R^{3+} ion did not lead to a substantial change in the structure. Thermodynamic properties of rare-earth francisites considerably differ within the family, depending on the ion entering the composition. The R^{3+} ions can be divided into two groups: with zero ($\mathbf{J} = 0$) and nonzero ($\mathbf{J} \neq 0$) magnetic moment. The first group includes francisites with ions Y [14], La [19], Eu, and Lu [17], the second group includes those with Sm [16], Yb [18], and Nd [15].

Temperature dependences of magnetic susceptibility of $Cu_3R(SeO_3)_2O_2Cl$ obtained in powder samples share a common feature; a sharp peak at $T_N = 30-40$ K (Table 3), corresponding to antiferromagnetic ordering. The presence of a phase transition is confirmed by measurements of specific heat and neutron diffraction, which revealed the inclined magnetic structure of $Cu_3Y(SeO_3)_2O_2Cl$ [14] similar to bismuth francisite [28]. Figure 14a presents the dependences of the magnetic susceptibility of $Cu_3Y(SeO_3)_2O_2Cl$ [14], measured in different magnetic fields with a magnitude up to 9 T. The corresponding dependences for other rare-earth francisites with nonmagnetic rare-earth ions look similar. A sharp peak is observed in the fields up to 1 T; in stronger fields, it broadens, and T_N shifts toward a lower temperature. In the paramagnetic region, the Curie–Weiss law can describe the temperature dependence of magnetic susceptibility with the parameters presented in Table 3. Positive Weiss temperatures Θ in all rare-earth francisites studied testifies to the predomination of ferromagnetic exchange interactions at high temperatures. The behavior of parameter C (inset in Fig. 14a) with a decrease in temperature evidences the enhancement of antiferromagnetic interactions in the system. For the $Cu_3Eu(SeO_3)_2O_2Cl$ compound, the temperature-dependent contribution of van Vleck's paramagnetism plays a significant role [17].

One more characteristic feature of bismuth francisite, metamagnetic transformation, was also observed in rare-earth francisites. Figure 14b presents magnetization loops for powder samples of $Cu_3Eu(SeO_3)_2O_2Cl$ and $Cu_3Lu(SeO_3)_2O_2Cl$, demonstrating a linear dependence in magnetic fields below the metamagnetic transition field and a sharp increase in stronger magnetic fields. The insets in this figure schematically present the magnetic structure: at $B < B_C$, the wavy kagome layers are ordered among themselves antiferromagnetically; at $B > B_C$, each second layer flips, and a total ferromagnetic order is established. The basic parameters of the magnetic subsystem of rare-earth francisites with R ions with a zero dipole moment are presented in Table 3.

Temperature dependences of magnetic susceptibility of francisites with rare-earth ions possessing a nonzero magnetic moment, $Cu_3R(SeO_3)_2O_2Cl$ (R = Sm, Yb, Nd), have a radically different form: besides the peak at $T_N = 30-40$ K, corresponding to antiferromagnetic ordering, additional

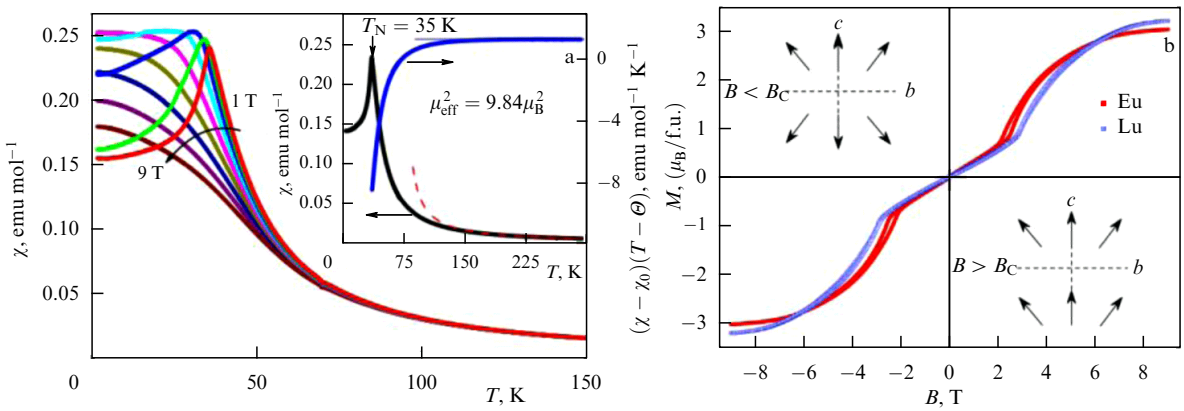

Figure 14. (a) Temperature dependences of $Cu_3Y(SeO_3)_2O_2Cl$ reduced magnetization in magnetic fields of 1–9 T [14]. Inset: temperature dependences of $Cu_3Y(SeO_3)_2O_2Cl$ magnetic susceptibility in a field of 0.1 T and the Curie constant C written if the form of a product $(\chi - \chi_0)(T - \Theta)$. The dashed line represents the Curie–Weiss law. (b) Metamagnetic phase transition in $Cu_3Eu(SeO_3)_2O_2Cl$ and $Cu_3Lu(SeO_3)_2O_2Cl$. Inset: schematic diagrams of orientation of copper ion magnetic moments in weak and strong magnetic fields [17].

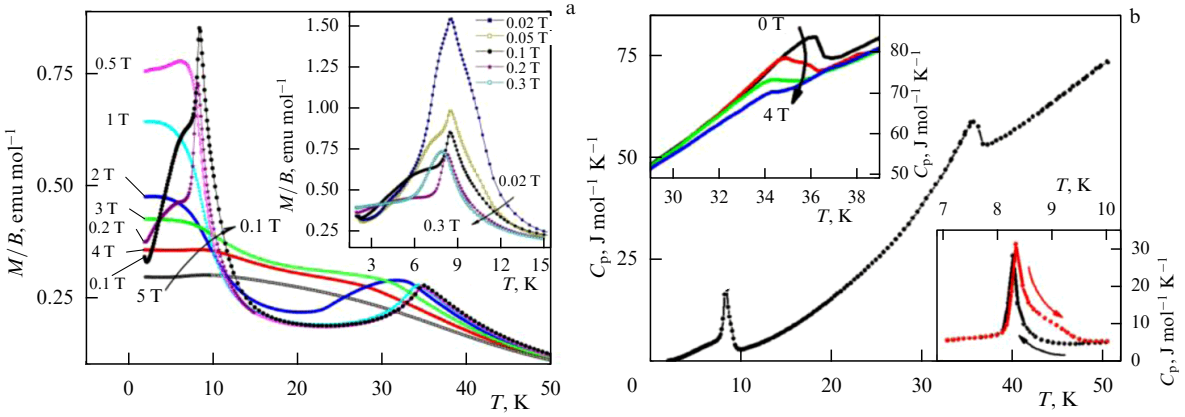

Figure 15. (a) Temperature dependences of $Cu_3Sm(SeO_3)_2O_2Cl$ reduced magnetization measured in various magnetic fields in the regime of cooling without a magnetic field [16]. The inset shows temperature dependences of $Cu_3Sm(SeO_3)_2O_2Cl$ magnetic susceptibility in weak magnetic fields near the temperature T_R of the spin-reorientation transition in the transition metal subsystem. (b) Temperature dependences of $Cu_3Yb(SeO_3)_2O_2Cl$ specific heat [18]. Upper inset — in various magnetic fields; lower inset — upon decreasing and increasing the temperature.

anomalies are observed at low temperatures [15, 16, 18]. These anomalies are related to spin reorientation of copper ions Cu^{2+}; however, this phase transition has a number of specific features for each rare-earth francisite. In $Cu_3R(SeO_3)_2O_2Cl$ (R = Sm, Nd), the spin reorientation at temperature T_R manifests itself as a sharp peak; in this case, as shown in Fig. 15a, in samarium francisite below this peak, a Schottky-type anomaly is observed, caused by the splitting of Sm^{3+} ion levels. In $Cu_3Yb(SeO_3)_2O_2Cl$, the phase transition manifests itself as a sharp increase in susceptibility, more typical of a first-order phase transition. The specific heat temperature dependences confirm the presence of phase transitions at T_R. In $Cu_3R(SeO_3)_2O_2Cl$ (R = Sm, Nd), at this temperature λ-type anomalies are observed, characteristic of a second-order phase transition. In $Cu_3Yb(SeO_3)_2O_2Cl$, a bright anomaly is present at 8.5 K (see Fig. 15b). This anomaly is suppressed by an external magnetic field, as shown in the upper inset. The lower inset illustrates the specific heat hysteresis behavior characteristic of a first-order phase transition.

The field dependences of magnetization in rare-earth francisites $Cu_3R(SeO_3)_2O_2Cl$ (R = Sm, Yb, Nd) substantially change at phase transitions. Figure 16 shows hysteresis loops $M(B)$ in $Cu_3Yb(SeO_3)_2O_2Cl$ at $T < T_R$ (2 K) and in the interval $T_R < T < T_N$ (10 and 20 K). At 2 K in weak fields, a ferromagnetic loop is observed in the dependence $M(B)$ with a considerable residual magnetization, the magnitude of which amounts to $\sim 1\ \mu_B$. At 10 K, the residual zero-field magnetization is absent, but narrow loops symmetric with respect to the origin of coordinates arise, corresponding to a metamagnetic transition in weak fields. Upon increasing the temperature to 20 K, the dependence $M(B)$ has a linear region for $B < B_C$, and the narrow loops accompanying the first-order transition are shifted to higher fields. At temperatures $T > T_N$, the hysteresis disappears, and the dependence $M(B)$ in the paramagnetic region becomes linear in weak fields.

The spin reorientation of copper ions Cu^{2+} in the compounds $Cu_3R(SeO_3)_2O_2Cl$ (R = Sm, Yb, Nd) is confirmed by the study of the temperature evolution of optical absorption spectra of R^{3+} ions. Figure 17 presents the optical spectra of francisites based on Sm^{3+} (a–d) [16] and Yb^{3+} (e–h) [18]. As shown in the lower panels of Fig. 17, two temperatures, T_N and T_R, at which the form of the lines is

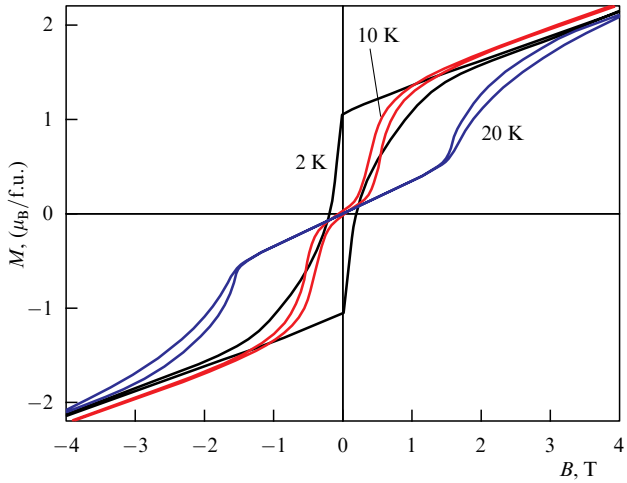

Figure 16. Field dependences of magnetization in $Cu_3Yb(SeO_3)_2O_2Cl$ at $T < T_R$ (2 K) and in the interval $T_R < T < T_N$ (10 and 20 K).

changed, are seen. Most lines in the spectra at T_N demonstrate a drastic narrowing; however, some of the lines split at this temperature. The Kramers doublet splitting unambiguously indicates the appearance of a local magnetic field, the ground Kramers doublet not splitting at T_N. The second and more clearly expressed specific feature in the temperature behavior of R^{3+} levels is located near T_R. At this temperature, all spectral lines are split; however, because of a fall in the population of the upper component of the split Kramers doublet at low temperatures, this feature looks like a shift to the region of higher energies. In $Cu_3Yb(SeO_3)_2O_2Cl$, this splitting is jump-like, and in the compounds $Cu_3R(SeO_3)_2O_2Cl$ (R = Sm, Nd) it occurs smoothly, which testifies to the first- and second-order phase transition, respectively.

In the low temperature range $T_R < T < T_N$, the francisites $Cu_3R(SeO_3)_2O_2Cl$ (R = Sm, Yb, Nd) are in a canted layered antiferromagnetic state with rare-earth ions located between the layers. Thus, the effective magnetic field B_{eff} acting from the copper subsystem on R^{3+} ions is directed along the crystallographic axis $c(z)$. The absence of splitting of the ground Kramers doublet of R^{3+} ion within the temperature interval $T_R < T < T_N$ testifies to the fact that

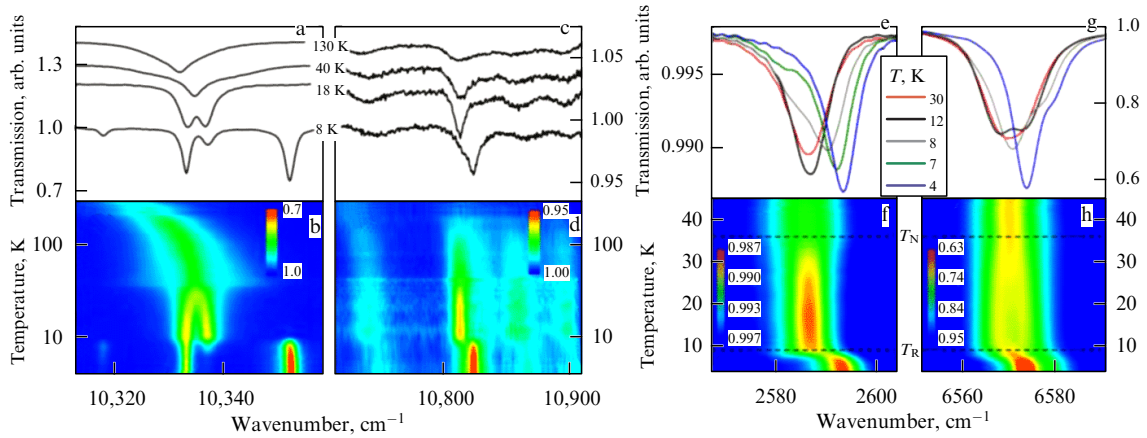

Figure 17. Characteristic absorption spectral lines of Sm^{3+} (a–d) [16] and Yb^{3+} (e–h) [18] ions at various temperatures (a, c, e, g) and temperature dependences of intensities of these spectral lines (b, d, f, h).

the z-component of its g-factor is close to zero. The splitting of the ground Kramers doublet occurring at temperatures below T_R is due to the B_{eff} rotation as a result of a spin-reorienting phase transition in the copper magnetic subsystem. This transition is caused by the increased magnetic anisotropy of the rare-earth ion. In Refs [16, 18], *ab initio* calculations of exchange interactions in the compounds $Cu_3R(SeO_3)_2O_2Cl$ (R = Y, Sm) were carried out. As in bismuth francisite, ferromagnetic exchange is dominant in the kagome layers of rare-earth francisites, while between the layers a significantly weaker antiferromagnetic exchange prevails.

In Refs [15, 19], in addition to the thermodynamic properties of oxochlorides $Cu_3R(SeO_3)_2O_2Cl$ (R = La, Nd), those of oxobromides of these compositions were also studied. Varying the halogen in these compounds caused no additional phase transformations, like the structure transition at $T_S = 115$ K in $Cu_3Bi(SeO_3)_2O_2Cl$. No structural phase transition was observed in other rare-earth francisites either. In the compounds $Cu_3Nd(SeO_3)_2O_2X$ (X = Cl, Br), a difference in the low-temperature anomaly at T_R was observed; in $Cu_3Nd(SeO_3)_2O_2Cl$, this anomaly vanished already in a magnetic field of 1 T, while in the bromide it persisted up to 3 T. Moreover, in the field dependence of magnetization in $Cu_3Nd(SeO_3)_2O_2Br$ at temperatures below T_R, no region of spontaneous magnetization was observed, unlike in other francisites with a low-temperature spin-reorientation transition.

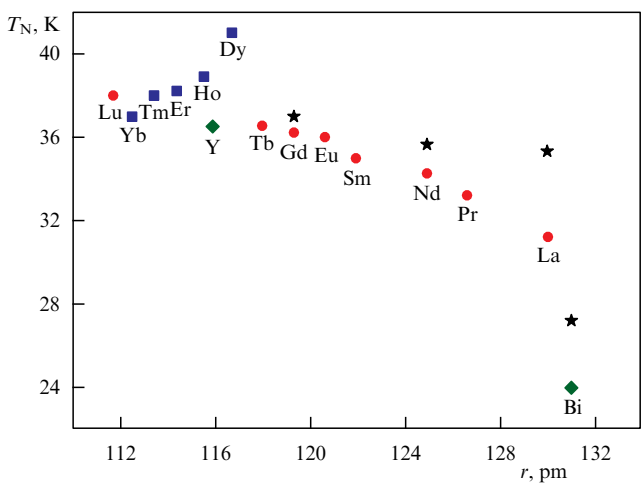

Figure 18. Dependence of magnetic ordering temperature on the rare-earth ion radius in the francisite family of compounds. Starts mark the ordering temperatures of bromide analogs of similar compositions.

Substitution of rare-earth ions R in the Bi position of the francisite structure is accompanied by a sharp increase in the temperature of magnetic ordering T_N. This is apparently due to the fact that the loose electron pair of bismuth plays the role of 'chemical scissors' in the structure of these compounds, affecting the parameters of exchange interaction. As shown in Fig. 18, the dependence of this temperature on the rare-earth ion radius r is nontrivial. First, upon proceeding from Yb to Dy, the value of T_N rapidly increases, and then, from Gd to La, this temperature monotonically decreases. The origin of such a behavior requires additional study.

9. Conclusion

Alongside some other minerals and compounds with an unusual magnetic subsystem topology [43–48], francisites belong to the most demanded quantum objects of condensed matter physics. This is due to both a unique chemical composition, allowing variations with respect to basic crystallographic positions, and a combination of unusual properties, manifesting themselves in various physical measurements. Ferromagnetic interactions dominate in the wavy kagome lattice of francisites. The competition of these interactions with next to nearest antiferromagnetic interactions leads to multisublattice ferrimagnetism, radically different from Lieb–Mattis ferrimagnetism [49]. An example of such ferrimagnetism is the umbrella-type structure in $Ni(NO_3)_2$ [50]. Under the action of a magnetic field, francisites undergo a metamagnetic transformation manifesting itself, in particular, in the broadband absorption of electromagnetic radiation. Upon a change in temperature, francisites undergo a structural transformation from a nonpolar *Pmmn* phase to a nonpolar *Pcmn* phase; however, at low temperatures, multiferroic effects are observed in francisites under the action of an external magnetic field. Substitution of rare earths in the bismuth position substantially changes the francisite magnetic properties; in some rare-earth francisites, spin-reorientation transitions with a decrease in temperature are observed. A number of aspects of the behavior of rare-earth francisites need advanced investigation. Particularly, in

experiments on elastic neutron scattering, it is planned to establish the magnetic structure of these materials, and, in theory, it could be useful to analyze spin-reorientation phase transitions observed in them.

Acknowledgments
This study was carried out with financial support from the Russian Foundation for Basic Research (project nos 19-12-50040, 19-33-60093, and 20-02-00015). KVZ expresses gratitude to the Russian Scientific Foundation for support (grant no. 19-42-02010). ANV thanks the Ministry of Science and Higher Education of the Russian Federation (contracts 02.A03.21.0004 and 02.A03.21.0011) and the National University of Science and Technology MISIS (grant no. K2-2020-008) for their support.

References

1. Grünbaum B, Shephard G C *Tilings and Patterns* (New York: W.H. Freeman, 1987)
2. Sun Y et al. *Nano Lett.* **17** 2771 (2017)
3. Tsirlin A A et al. *Phys. Rev. B* **87** 064404 (2013)
4. Meyer J C et al. *Nature* **446** 60 (2007)
5. Taniguchi S et al. *J. Phys. Soc. Jpn.* **64** 2758 (1995)
6. Môri N et al. *Physica B* **239** 137 (1997)
7. Kageyama H et al. *Phys. Rev. Lett.* **82** 3168 (1999)
8. Han T-H et al. *Nature* **492** 406 (2012)
9. Francis G L *Minerals of Iron Monarch* (Whyalla, SA: Onesteel, 2010)
10. Pring A, Gatehouse B M, Birch W D *Am. Miner.* **75** 1421 (1990)
11. Millet P et al. *J. Mater. Chem.* **11** 1152 (2001)
12. Becker R, Johnsson M *Solid State Sci.* **7** 375 (2005)
13. Berdonosov P S, Dolgikh V A *Russ. J. Inorg. Chem.* **53** 1353 (2008); *Zh. Neorg. Khim.* **59** 1451 (2008)
14. Zakharov K V et al. *Phys. Rev. B* **90** 214417 (2014)
15. Markina M M et al. *J. Magn. Magn. Mater.* **492** 165721 (2019)
16. Zakharov K V et al. *Phys. Rev. B* **94** 054401 (2016)
17. Zakharov K V et al. *J. Alloys Compd.* **685** 442 (2016)
18. Markina M M et al. *Phys. Rev. B* **96** 134422 (2017)
19. Markina M M et al. *Phys. Chem. Min.* **44** 277 (2017)
20. Berrigan R, Gatehouse B M *Acta Cryst. C* **52** 496 (1996)
21. Nazarchuk E V et al. *Phys. Chem. Min.* **27** 440 (2000)
22. Milesi-Brault C et al. *Phys. Rev. Lett.* **124** 097603 (2020)
23. Tolédano P, Guennou M *Phys. Rev. B* **94** 014107 (2016)
24. Kittel C *Phys. Rev.* **82** 729 (1951)
25. Levitin R Z, Markosyan A S *Sov. Phys. Usp.* **31** 730 (1988); *Usp. Fiz. Nauk* **155** 623 (1988)
26. Prishchenko D A et al. *Phys. Rev. B* **95** 064102 (2017)
27. Gnezdilov V et al. *Phys. Rev. B* **96** 115144 (2017)
28. Constable E et al. *Phys. Rev. B* **96** 014413 (2017)
29. Oliver S R J *Chem. Soc. Rev.* **38** 1868 (2009)
30. Miller K H et al. *Phys. Rev. B* **86** 174104 (2012)
31. Pregelj M et al. *Phys. Rev. B* **86** 144409 (2012)
32. Palstra T T M et al. *Phys. Rev. B* **31** 4622 (1985)
33. Kunesh C J, Narasimhan K S, Butera R A *J. Phys. Chem. Solids* **34** 2003 (1973)
34. Rousochatzakis I et al. *Phys. Rev. B* **91** 024416 (2015)
35. Nikolaev S A et al. *Phys. Rev. B* **94** 144412 (2016)
36. Olariu A et al. *Phys. Rev. Lett.* **100** 087202 (2008)
37. Norman M R *Rev. Mod. Phys.* **88** 041002 (2016)
38. Wang Z et al. *Phys. Rev. B* **86** 174411 (2012)
39. Pregelj M et al. *Adv. Funct. Mater.* **25** 3634 (2015)
40. Zorko A et al. *AIP Adv.* **6** 056210 (2016)
41. Wu H C et al. *J. Phys. D* **50** 265002 (2017)
42. Tokunaga Y et al. *Phys. Rev. Lett.* **101** 097205 (2008)
43. Sobolev A V et al. *J. Phys. Chem. C* **122** 19746 (2018)
44. Koshelev A V et al. *Phys. Rev. Appl.* **10** 034008 (2018)
45. Rahaman B et al. *Phys. Rev. B* **98** 044412 (2018)
46. Nalbandyan V B et al. *Dalton Trans.* **47** 14760 (2018)
47. Gnezdilov V P et al. *Phys. Rev. B* **99** 064413 (2019)
48. Inosov D S *Adv. Phys.* **67** 149 (2018)
49. Lieb E, Mattis D *J. Math. Phys.* **3** 749 (1962)
50. Volkova O S et al. *Phys. Rev. B* **90** 134407 (2014)